

Free Trions with Near-Unity Quantum Yield in Monolayer MoSe₂

Bumho Kim, Yue Luo, Daniel Rhodes, Yusong Bai, Jue Wang, Song Liu, Abraham Jordan, Baili Huang, Zhaochen Li, Takashi Taniguchi, Kenji Watanabe, Jonathan Owen, Stefan Strauf, Katayun Barmak,* Xiaoyang Zhu,* and James Hone*



Cite This: *ACS Nano* 2022, 16, 140–147



Read Online

ACCESS |



Metrics & More



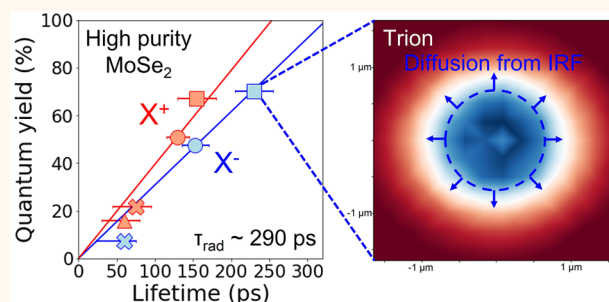
Article Recommendations



Supporting Information

ABSTRACT: Trions, quasiparticles composed of an electron–hole pair bound to a second electron and/or hole, are many-body states with potential applications in optoelectronics. Trions in monolayer transition metal dichalcogenide (TMD) semiconductors have attracted recent interest due to their valley/spin polarization, strong binding energy, and tunability through external gate control. However, low materials quality (*i.e.*, high defect density) has hindered efforts to understand the intrinsic properties of trions. The low photoluminescence (PL) quantum yield (QY) and short lifetime of trions have prevented harnessing them in device applications. Here, we study the behavior of trions in a series of MoSe₂ monolayers, with atomic defect density varying by over 2 orders of magnitude. The QY increases with decreasing defect density and approaches unity in the cleanest material. Simultaneous measurement of the PL lifetime yields both the intrinsic radiative lifetime and the defect-dependent nonradiative lifetime. The long lifetime of ~230 ps of trions allows direct observation of their diffusion.

KEYWORDS: transition metal dichalcogenide, MoSe₂, trion, quantum yield, intrinsic lifetime, diffusion



INTRODUCTION

As atomically thin direct-gap semiconductors,¹ monolayer TMDs are promising for a broad range of optical and optoelectronic applications. In monolayer TMDs, strong electron–hole interaction due to quantum confinement and reduced dielectric screening² produces strongly bound composite quasiparticles, including excitons, trions,^{3,4} biexcitons,^{5–11} and charged biexcitons.^{5,9–11} The trion with valley and spin polarization is of particular interest for applications in valleytronics, spintronics, light emitters, and photodetectors. Trions can be manipulated by external electric fields,¹² which can potentially be used to achieve efficient energy transfer and realize a trion-valley Hall effect.¹³

In spite of this considerable interest, many fundamental properties of trion such as the radiative and nonradiative lifetimes and diffusivity have not been well established. More broadly, there is disagreement in the theoretical literature as to the nature of the trion. The trion has been interpreted as a three-body charge–exciton bound state.^{3,4,14} However, recent theoretical work has suggested that trion is a charge neutral bosonic particle described by an exciton polaron in a Fermi sea,^{15–17} a superposition of an exciton state and a four-body state consisting of an exciton bound to a conduction band

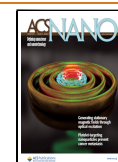
(CB) electron and a CB hole¹⁸ or bound-states from electron–exciton scattering.¹⁹ Moreover, recent work has proposed that defect-bound excitons may be responsible for the low energy PL features assigned as free trions at low doping density.²⁰

The models above predict very different radiative lifetimes and diffusivity, but the quantities have not been determined experimentally. In this regard, materials quality has been the major obstacle to progress; most studies have utilized TMDs with high (10^{12} – 10^{13} cm^{−2}) defect density, in which the QY is low.^{1,21–25} (see Supporting Information, Table S1). In such materials, the experimentally determined lifetime is only in the tens of ps range at cryogenic temperatures.^{26–28} Higher-purity materials are required for measurement of an intrinsic radiative lifetime and to determine whether trions are freely diffusing species. For instance, the long lifetime (above 100 ps) of trions in GaAs quantum wells (QWs) allows for the observation of

Received: May 21, 2021

Accepted: December 16, 2021

Published: December 22, 2021



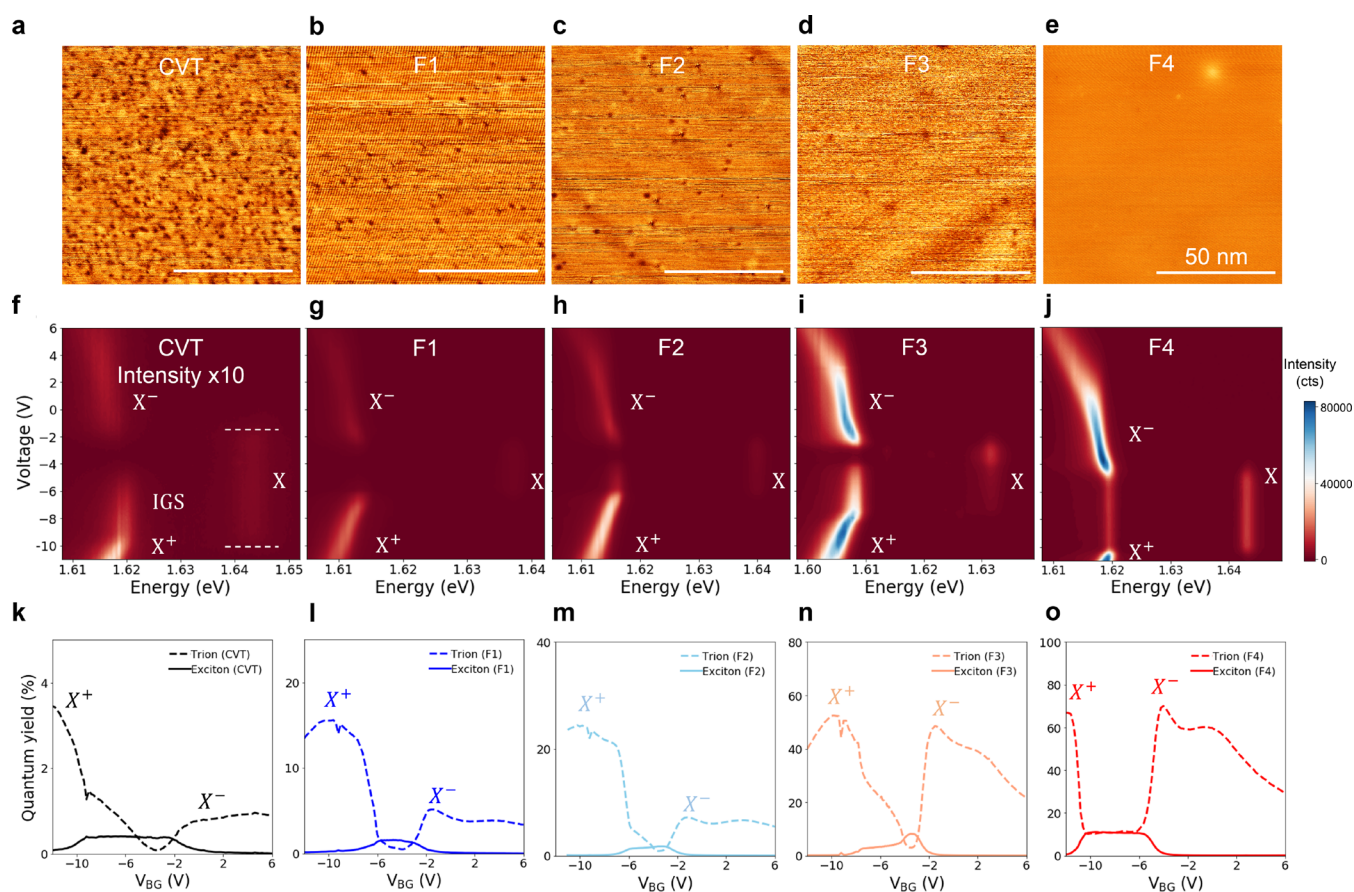


Figure 1. Characterization of defects and gate-dependent quantum yield of CVT and flux-grown MoSe₂. (a) STM topographic images of CVT-grown MoSe₂ and (b–e) flux-grown MoSe₂ with different growth parameters (F1, F2, F3, and F4). The STM measurements were performed with $V = 1.0$ V, $I = 150$ pA. The scale bar in the STM topographic images represents 50 nm. PL color plot as a function of the gate bias of (f) CVT-grown MoSe₂, and (g–j) flux-grown MoSe₂ with different defect densities. For the PL color map, the samples were excited using a continuous-wave (CW) laser with an excitation wavelength of 532 nm at 4K. The intensity of gate-dependent color plot for CVT-grown MoSe₂ was multiplied by 10 for clarity. Thickness of the bottom *h*-BN used for CVT, F1, F2, F3, and F4 samples are 29, 23, 36, 33, and 35 nm, respectively. The gate-dependent quantum yield for (k) CVT, (l) F1, (m) F2, (n) F3, and (o) F4 samples. Dashed lines and solid lines represent quantum yield for trion and exciton, respectively.

trion diffusion up to ~ 1 μm at 4K, firmly establishing that trions in QWs are mobile species.²⁹ To date, the only diffusion measurements of trions in monolayer TMDs have been performed in WS₂ and WSe₂,^{30,31} where dark states can act as a long-lived reservoir for energy. In MoSe₂, the lowest-energy states are bright, making it a more appropriate material in which to directly determine the nature and behavior of trions in TMDs.

In this work, we study low-temperature PL of monolayer MoSe₂ derived from crystals with defect densities ranging from $5 \times 10^{12} \text{ cm}^{-2}$ to $8 \times 10^{10} \text{ cm}^{-2}$, which have been independently measured by scanning tunneling microscopy (STM). In these samples, we measure the quantum yield and lifetime of the trion state, focusing on the low doping density regime. The trion QY increases dramatically with decreasing defect density, reaching values near unity. Time-resolved measurements provide the measurement of both the intrinsic radiative lifetime of ~ 290 ps and the defect-dependent nonradiative lifetime, which exceeds that of the exciton by 2–3 orders of magnitude. This long lifetime allows observation of trion diffusion, conclusively establishing that trions are mobile species. This work shows that nonradiative recombination of trions at defects is inefficient compared to that of excitons.

RESULTS AND DISCUSSION

Parts a–e of Figure 1 show STM images of MoSe₂ crystals cleaved *in vacuo*. In these images, single-atom point defects acting as acceptor and donor states are seen as dark and bright spots, respectively. The effect of these defects on the local density of states extends over many lattice sites, allowing for large-scale imaging and accurate estimation of the defect density.³² Figure 1a shows an image of MoSe₂ grown by chemical vapor transport (CVT), the most commonly utilized method for single-crystal TMD synthesis. Consistent with previous studies,^{32–34} the density of donor/acceptor defects in CVT-grown MoSe₂ is high, approximately $(5 \pm 3 \times 10^{12} \text{ cm}^{-2})$. Parts b–e of Figure 1 show STM images of MoSe₂ crystals grown by a self-flux technique. These crystals (labeled F1, F2, F3, and F4) were each grown with slightly different parameters and have defect densities of $(6 \pm 2 \times 10^{11} \text{ cm}^{-2})$, $(5 \pm 1 \times 10^{11} \text{ cm}^{-2})$, $(3 \pm 1 \times 10^{11} \text{ cm}^{-2})$, and $(8 \pm 5 \times 10^{10} \text{ cm}^{-2})$, respectively (see Methods for details of crystal growth and STM imaging).

For optical studies, monolayers are extracted from these crystals by mechanical exfoliation and encapsulated with hexagonal boron nitride (*h*-BN) to minimize external disorder.^{35,36} Because the optical response depends strongly

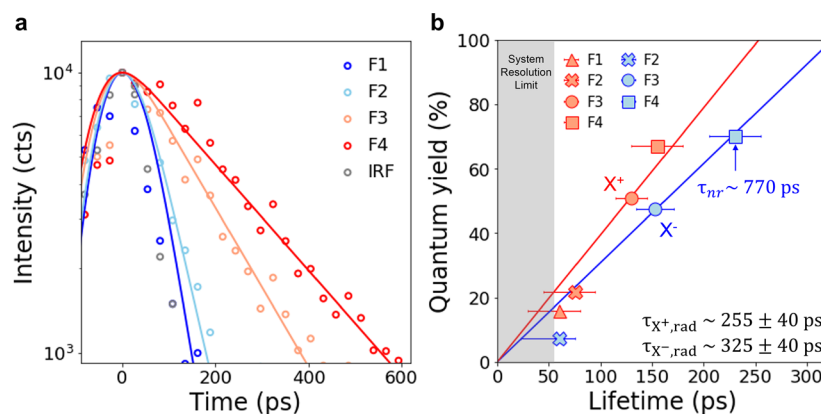


Figure 2. Intrinsic lifetime and quantum yield of trions in MoSe₂. (a) Time-resolved PL of flux-grown monolayer MoSe₂ with different defect densities. The time-resolved PL was performed for trions at the electron density of $3 \pm 2 \times 10^{11} \text{ cm}^{-2}$ for F1, F2, F3, and F4. For the time-resolved PL, the samples were excited using a pulsed laser with a repetition frequency of 78 MHz and an excitation wavelength of 700 nm at 4 K (see Methods). The trion decays (circles) were fitted with a convolution (lines) of a Gaussian and an exponential decay (see Methods). IRF denotes the instrument response function. (b) quantum yield vs lifetimes of flux-grown MoSe₂. Red and blue markers with error bars represent quantum yield and lifetime data of the positive trion and the negative trion at low doping density ($<1 \times 10^{12} \text{ cm}^{-2}$) (Methods). The quantum yield and lifetime data can be seen in Figure 1 and Supporting Information, Table S2.

on the charge state, the samples are contacted with graphite electrodes and placed on a thick gold back-gate to allow electrostatic control of carrier density. The gold also acts as a back reflector for direct measurement of the quantum yield (QY), where a diluted R6G dye is used as in refs 1, 21, and 24 (see Supporting Information, section 1).

Parts f–j of Figure 1 show the low-temperature (4 K) gate-dependent PL response of MoSe₂ monolayers derived from the crystals in Figure 1a–e (with bottom *h*-BN thickness ranging from 20 to 30 nm as noted). The observed behavior is consistent with previous studies:^{3,37} the neutral exciton PL at 1.64 eV appears in a finite range of negative gate voltages, indicated by the dashed lines. We take this as the range over which the chemical potential is inside the gap of the MoSe₂. In these samples, the width of the gap is strongly dependent on contact resistance (see Supporting Information, Figures S12 and S13). Outside of the gap, PL from the trion states appears, with a binding energy of $\sim 26 \pm 1$ meV relative to the exciton. Although the nature of trion is still an ongoing controversy, here we use the conventional notation of X⁺ and X[−] to label the trion states that appear when the Fermi level is in the valence and conduction bands, respectively. For simplicity, we refer to the trion states as “trions” below. As in previous studies, the trion peaks down-shift with increasing electron or hole doping.^{37,38} The electrostatic doping density was estimated using a parallel plate capacitor model (see Supporting Information, section 2). This red-shift with doping density has been attributed to band gap renormalization³⁹ and also has been explained by the exciton–polaron¹⁵ and exciton–trion superposition models.^{18,19} In previous studies of monolayer MoSe₂ on SiO₂, a broad emission peak ~ 65 meV below the exciton was observed within the gap regime.³ This feature is not present in the *h*-BN-encapsulated monolayers, implying that the low energy emission originates from excitons bound to charged defects in the substrate. Here, we instead observe emission within the gap regime at energy similar to that of the trions outside the gap. This in-gap state (IGS) may be due to the presence of excitons bound to charged defects in the MoSe₂ rather than the substrate (see Supporting Information, section 6) but may also be a phonon replica of

the exciton state. Further study is needed to understand the nature of this state.

Whereas the energy and gate-tunability of the PL spectra are roughly similar for all five samples, the intensity of all of the features dramatically increases with decreasing defect density. Parts k–o of Figure 1 show the integrated QY as a function of gate voltage for the exciton and trion states in these five samples. In all samples, the trion QY exceeds that of the exciton. For the CVT-grown sample, the peak trion quantum yield is $\sim 3.6\%$ (see Figure 1k), consistent with previous reports.^{21,22} This low QY indicates that nonradiative recombination is dominant. The peak quantum yields of the X⁺ trion are 16%, 22%, 52%, and 67% for samples F1, F2, F3, and F4, respectively (see Figure 1l–o). The F4 sample shows even higher peak quantum yield (70%) for the X[−] trion. High trion QY is rare in any material, with colloidal quantum dots showing the highest reported value of 46 %, while the highest value for TMDs has been 3.2% (see Supporting Information, Table S1). The trion PL intensity shows linear power-dependence for laser irradiance ranging from 1×10^{-3} to $4 \times 10^1 \text{ W/cm}^2$, such that the QY is nearly constant (see Supporting Information, Figure S7).

We next examine how reducing the defect density affects the trion lifetime. We measure lifetime just outside of the gap regime at low doping density, where the trion QY is highest and where the coupling strength in the exciton–trion superposition model is predicted to be weakest.^{18,40} Figure 2a shows time-resolved photoluminescence (TRPL) spectra of negative trions ($n \sim 3 \pm 2 \times 10^{11} \text{ cm}^{-2}$) measured by time-correlated single photon counting (TCSPC), for samples F1, F2, F3, and F4. The measured lifetime (τ_{TRPL}) was extracted by fitting the trace with a convolution of exponential decay and a Gaussian function representing the detector time-response (see Methods). With decreasing defect density, τ_{TRPL} increases, reaching ~ 230 ps for F4. The measured lifetime for the CVT-grown monolayer is within the system resolution limit (~ 49 ps; see Methods), consistent with the previously reported lifetime of ~ 15 ps.^{26,41} The observed PL linewidth of ~ 1.7 meV is more than 2 orders of magnitude greater than the linewidth limited by the TRPL lifetime (see Supporting Information, section 7). This implies that the linewidth may be

limited by pure dephasing time (T_2) rather than the population decay time (T_1). The extracted lower bound of pure dephasing time is ~ 0.78 ps, consistent with previous studies.^{42,43} As shown in Figure 2b, the measured trion QY increases with τ_{TRPL} for the four flux-grown samples. From the measured lifetime and quantum yield, it is straightforward to determine both the radiative lifetime τ_r and the nonradiative lifetime τ_{nr} according to

$$\text{QY} = \frac{\tau_r^{-1}}{\tau_r^{-1} + \tau_{\text{nr}}^{-1}} = \frac{\tau_r^{-1}}{\tau_{\text{TRPL}}^{-1}} \quad (1)$$

The solid lines show best-fit lines, corresponding to radiative lifetimes of $\tau_r = (325 \pm 40)$ ps for X^- and (255 ± 40) ps for X^+ . The validity of these parameters across four different samples, as well as the high measured QY, provides strong evidence that the derived radiative lifetimes are intrinsic and independent of material quality. The observed intrinsic lifetimes are in agreement with theoretical predictions of the three-body trion model.⁴⁴ More recent analysis predicts strongly momentum-dependent radiation, with fast (\sim ps) recombination inside the light cone and slower (a few hundred ps) recombination outside.⁴⁰ Comparison of these predictions to the values measured here will require further analysis to understand the effects of ensemble averaging. We also note that TRPL measurements with ps-level time resolution should be able to observe the predicted fast recombination directly. Interestingly, the measured lifetime is 2 orders of magnitude larger than the radiative lifetime of the neutral exciton (~ 2 ps^{26,45}) as observed by TRPL. Thus, the observed higher quantum yield for trions compared to excitons implies that the nonradiative lifetime of trions is much longer than that of excitons (with the important caveat that measurements are taken with the sample at different charge densities). In fact, τ_{nr} is comparable to τ_r for sample F3 and reaches ~ 770 ps for sample F4. We revisit this issue in Figure 4 below.

The open question of whether trions in 2D TMDs are free or defect-bound species can be directly addressed by measuring trion diffusion.²⁹ Critically, such measurements require trion lifetimes long enough to allow for diffusion away from the laser spot, a challenge that has hindered previous efforts but can be overcome using the higher purity, lower defect density MoSe₂ studied here. We observe trion diffusion in sample F4, which has the lowest defect density by mapping spatial PL profiles under continuous illumination (see Supporting Information, Figure S8). For the diffusion measurement, low fluence of ~ 43 W/cm² was used to minimize heating. This laser fluence produces a low trion density of $\sim 4 \times 10^9$ cm⁻², so that electrostatic repulsion and other many-body effects can be neglected (see Supporting Information, section 4). Parts a–c of Figure 3 show PL maps of the IGS, X^- and X^+ trions. The IGS state shows spot size indistinguishable from that of the reflected laser, indicating that it can be an immobile defect-bound state (see Supporting Information, section 6). Therefore, we use the IGS profile to characterize the instrument response function. The PL maps of the X^- and X^+ show clear spreading compared to the IGS. To more quantitatively determine the distribution, we radially average the data and plot the intensity vs radial distance r (Figure 3d) and fit the data to a 2D Gaussian distribution $I = I_0 \exp(-r^2/r_0^2)$. The extracted values of r_0 for X^- (1.12 ± 0.04 μm) and X^+ (1.08 ± 0.05 μm) are larger than that of the IGS (0.86 ± 0.05 μm), which provides a lower bound on the

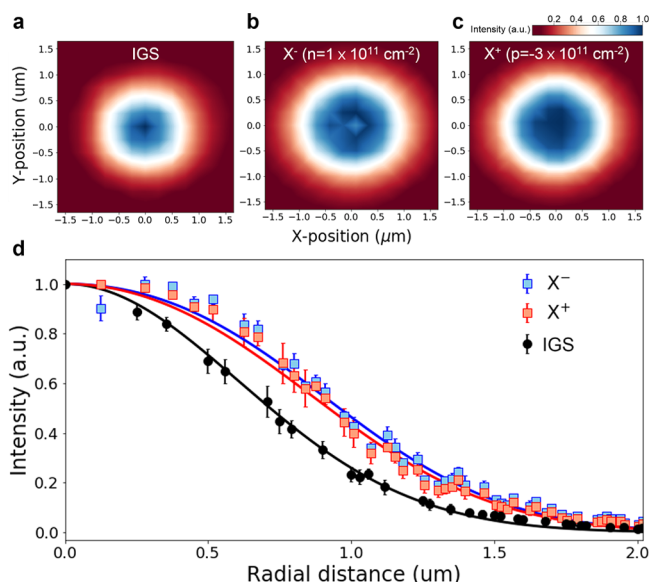


Figure 3. Spatial diffusion of trions. (a) Normalized spatial map of the IGS PL emission (b) the X^- PL emission at the electron density of 1×10^{11} cm⁻² (c) and X^+ PL emission at the hole density of -3×10^{11} cm⁻² in F4 sample. (d) Intensity vs radial distance profiles of IGS (black dots), X^- (blue dots) and X^+ (red dots) are extracted from the spatial maps. The intensities (dots) and errors (error bars) are the average and standard deviation of data from the spatial maps with the same radial distance from the center of illumination.

diffusion length of ~ 240 nm. Thus, unlike the IGS, the X^+ and X^- species in the doped regime show clear evidence of diffusion. A second flux-grown sample (F5) with higher defect density (see Supporting Information, Figures S9 and S10) exhibits a shorter diffusion length (~ 150 nm), highlighting the need for low defect density and long lifetime to observe trion diffusion.

In the low-density limit and steady-state condition, trion diffusion can be modeled using a simple two-dimensional diffusion equation:²⁹

$$D\nabla^2 n(r) + G(r) - \frac{n(r)}{\tau} = 0 \quad (2)$$

where D is the diffusion coefficient (cm²/s), $n(r)$ is the trion density (cm⁻²), $G(r)$ is the density of trions generated per unit time (cm⁻²s⁻¹), and τ is the trion lifetime (s). The resulting PL profiles are well described by this model (Figure 3d), which yields diffusion coefficients of (4.5 ± 0.6) cm²/s for X^- and (5.7 ± 1.2) cm²/s for X^+ (see Supporting Information, section 4). The diffusion length and extracted diffusion constants are within a factor of 6 of those trions in GaAs quantum wells at cryogenic temperatures (~ 1 μm and 30 cm²/s, respectively).²⁹ Thus, we can conclude that the positive and negative trions are free particles rather than defect-bound excitons. Further experimental studies (e.g., transport measurements or Shubnikov de Haas measurements⁴⁶) are required to discriminate between the trion and the Fermi polaron (or the exciton–trion superposition) models.

Nonradiative decay of trions in TMDs has not yet been addressed in theory or experiment. The results described in Figure 2 above establish that the trion quantum yield increases with decreasing defect density and can approach unity. These observations imply that the nonradiative trion lifetime is

limited by defects and can exceed the radiative lifetime in sufficiently clean samples. Figure 4 plots τ_{nr} vs defect density

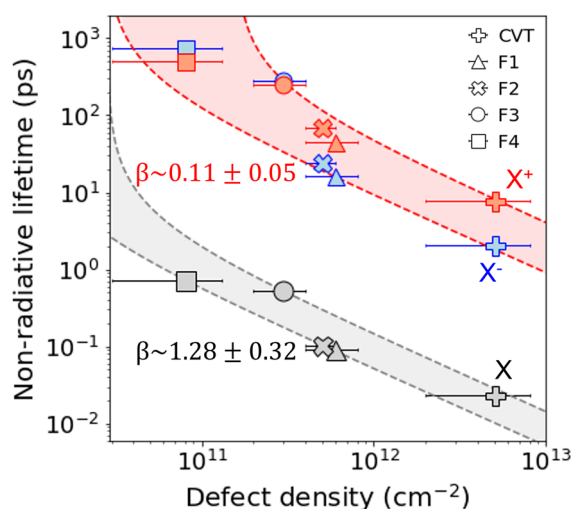


Figure 4. Defect-dependent nonradiative lifetime of exciton and trion in MoSe₂. Nonradiative lifetime vs defect density for CVT, F1, F2, F3, and F4 samples. The horizontal error bars represent the standard deviation of defect density of each sample. The nonradiative lifetimes were fitted with a diffusion model with β values of 0.11 ± 0.05 (red shaded area) and 1.28 ± 0.32 (gray shaded area) for trions and excitons, respectively (see Supporting Information, section 5). Upper and lower bounds of β are indicated by dashed lines.

for the five samples shown in Figure 1. Fixed hole ($5 \pm 2 \times 10^{11} \text{ cm}^{-2}$) and electron ($3 \pm 2 \times 10^{11} \text{ cm}^{-2}$) doping densities are chosen for the positive and negative trions, where the trion intensities are near their maximum values. For excitons, maximum exciton QY in the gap regime is used. We note that although we cannot directly measure the trion lifetime τ_{TRPL} for the CVT-grown sample, its nonradiative lifetime can be estimated from the quantum yield and the measured intrinsic τ_r obtained in Figure 2. Likewise, the nonradiative lifetime of the neutral exciton can be estimated from the measured QY and the theoretically predicted radiative lifetime.⁴⁷

For both trions and excitons, τ_{nr} increases with decreasing defect density (Figure 4). This is direct evidence of nonradiative recombination at defects for both species. For negative trions, τ_{nr} varies from ~ 2 ps for the CVT-grown sample to ~ 280 ps for sample F3, reaching 770 ps in sample F4 (Figure 4), a change of 2 orders of magnitude from the extrinsic limit ($\tau_{\text{nr}} \ll \tau_r$) and into the intrinsic limit ($\tau_{\text{nr}} > \tau_r$). The observed power-independent QY indicates similarly constant τ_{nr} . This implies that the defect-dependent nonradiative decay of trions may be dominated by defect-mediated Auger recombination (see Supporting Information, section 3). A similar increase of τ_{nr} with decreasing defect density is seen for the neutral excitons. Notably, however, the exciton nonradiative lifetime is 2–3 orders of magnitude smaller than that of the trions for the same defect density. Having established above that trions are free particles like excitons, we connect lifetime to quantum yield using a simple diffusion model. In this model, a fitting parameter β represents the ratio of mean defect spacing to diffusion length and reflects the probability of nonradiative decay at a given defect (see Supporting Information, section 5). This model can be broadly applied to defect-dependent nonradiative recombination (e.g.,

defect-mediated Auger recombination) of freely diffusing species (e.g., excitons and trions) in two dimensions. For both excitons and trions, the data across the five samples fit this model well. The extracted value of β is near unity for excitons, while β for trions is around 0.1, indicating much less efficient recombination at defects. Slower recombination is expected when the sample is charged (and trions are present) due to filling of trap states and screening by free carriers, but more detailed theoretical analysis is needed for a quantitative understanding of this difference.

CONCLUSIONS

This work experimentally demonstrates that trions in the doped regime in MoSe₂ are free particles with long radiative lifetime. The resistance of trions to nonradiative decay allows trions to achieve quantum yield near unity in samples with sufficiently low defect density and to diffuse for distances much longer than the average defect spacing. This high quantum yield is fundamentally distinct from the near-unity exciton quantum yield achieved at room temperature through chemical treatment of TMDs,²⁴ which arises due to thermal excitation of excitons out of long-lived dark states.⁴⁸ The high-quality MoSe₂ used in the current study provides a platform to explore a wealth of trion physics requiring long lifetime, including trion-valley Hall effect, confinement within Moire potentials, and steering of trions with applied electric fields. The high quantum yield and suppressed electron–hole recombination observed here will enhance the performance of many proposed optoelectronic devices, including light emitters^{49,50} and photodetectors.⁵¹

METHODS

Crystal Growth. Flux-grown MoSe₂ single crystals were prepared by combining Mo powder (Alfa Aesar, 99.999%) and Se shot (Alfa Aesar, 99.999+%) in a ratio of 1:50 (F1) and 1:100 (F2, F3, F4, and F5) at the bottom of a quartz ampule. A wad of quartz wool was placed in the middle of the quartz ampules for F1, F2, F3, and F5. No quartz wool was used for F4. The ampules were subsequently purged with Ar gas and sealed under vacuum ($\sim 5 \times 10^{-6}$ Torr). The quartz ampules with the reagents were placed vertically in a box furnace. For F1, the reagents were heated with a ramp rate of 40 °C/h to 1080 °C and held at 1080 °C for 366 h before cooling to 350 °C at a rate of 2.2 °C/h. For F2, the reagents were heated at 40 °C/h to 1080 °C, held at 1080 °C for 672 h, and cooled to 350 °C at 2.2 °C/h. For F3, the reagents were heated at 40 °C/h to 1000 °C, held at 1000 °C for 168 h, cooled to 600 °C at 1 °C/h, and then cooled to 380 °C at 4.6 °C/h. For F4, the reagents were heated with a ramp rate of 20 °C/h to 1000 °C held at 1000 °C for 168 h, then cooled to 600 °C at 1 °C/h, and then to 100 °C at 5 °C/h. For F5, the reagents were heated at 40 °C/h to 1000 °C held at 1000 °C for 336 h, then cooled to 600 °C at 1 °C/h and to 350 °C at 5.2 °C/h. After synthesis, F1, F2, F3, and F5 were taken out from the furnace, and the Se-flux in the ampules was decanted through the wad of quartz wool in a centrifuge. F4 crystals were taken out with excess Se and sealed in a new ampule with a wad of quartz wool at the center. The new ampule with F4 crystals with excess Se was heated to 350 °C, and then molten Se was decanted through the quartz wool in a centrifuge. The subsequently obtained 2H-MoSe₂ crystals (F1, F2, F3, F4, and F5) were placed at an end of a new quartz ampule sealed under vacuum (5×10^{-6} Torr). 2H-MoSe₂ crystals are positioned at a hot zone (250 °C) and the other side of the ampule is placed at a cold zone (50 °C) of a tube furnace for 48 h to remove any residual selenium. Commercially available CVT-grown MoSe₂ (HQ graphene) was used for the STM and optical characterization.

Scanning Tunneling Microscopy. STM measurements were performed using a Scienta Omicron STM system at room temperature

under an ultrahigh vacuum (base pressure $<2.0 \times 10^{-10}$ Torr). MoSe₂ bulk single crystals were mounted onto a metallic sample holder with silver epoxy and then cleaved *in vacuo* in the UHV STM chamber to obtain a clean surface. The tungsten tip was cleaned on a gold surface and calibrated on a graphite surface. For the defect density of MoSe₂ samples, we counted the number of defects and divided it by the scan area. For reliable estimation of defect density, we obtained 5 (25×25 nm²), 29 (50×50 nm²), 16 (50×50 nm²), 21 (50×50 nm²), and 20 (50×50 nm²) STM topographic images from CVT, F1, F2, F3, and F4 samples, respectively. The average and standard deviation values of defect densities from the topographic images are provided in the main text.

Stacking and Fabrication of Heterostructures. Monolayer MoSe₂ (CVT crystals from HQ graphene and home-grown flux crystals), graphite, and *h*-BN were exfoliated onto SiO₂/Si substrates. Top *h*-BN was picked up with a polydimethylsiloxane (PDMS) stamp coated with a polycaprolactone (PCL) polymer.⁵² The top *h*-BN on the polymer stamp was then used to pick up graphite top contact, monolayer MoSe₂, and bottom *h*-BN. Once the *h*-BN/graphite/MoSe₂/*h*-BN stack on the polymer was transferred onto a bottom gold back-gate electrode by melting the PCL, the stack was rinsed with acetone. The graphite edge-contact technique⁵³ was used for ground electrodes because the edge contacts provide the most straightforward way to make contact to encapsulated materials with high yield. The graphite edge-contact and large metal electrodes were fabricated using conventional electron-beam lithography followed by CHF₃/O₂ reactive ion etching to expose the edges of the graphite. Cr/Pd/Au were then deposited by electron-beam metal deposition to make edge contact to the top graphite.

Optical Characterization under Continuous Illumination. A CW laser with a wavelength of 532 nm was used for excitation to measure the gate-tunable PL (Figure 1f–j and Supporting Information, Figures S11 and S12), QY (y-axis in Figure 1k–o and 2b), spatial PL profile (Figure 3 and Supporting Information, Figure S10), absorbance (Supporting Information, Figures S1, S2, and S5), and power-dependent PL (Supporting Information, Figures S7 and S11).

Time-resolved Photoluminescence on Monolayer MoSe₂. Time-resolved photoluminescence (TRPL) was performed inside a closed-cycle cryogen-free cryostat (attodry1100 from attocube) with a base temperature of 4 K. The MoSe₂ samples were excited by a supercontinuum laser (NKT photonics) with a repetition frequency of 78 MHz and 7 ps pulse width. The wavelength of the laser is filtered by a 10 nm bandpass filter centered at 700 nm. TRPL was carried out with a TCSPC with a time bin resolution of 27 ps and a fast avalanche photodiode (APD) with a timing resolution of 40 ps (ID100 from IDQuantique). A system resolution limit is determined by error propagation formula ($\epsilon = \sqrt{(7 \text{ ps})^2 + (27 \text{ ps})^2 + (40 \text{ ps})^2} \sim 49 \text{ ps}$). The instrument response function (IRF) was acquired by measuring the reflected laser from the gold substrate. The IRF is well fitted with the Gaussian function with a full width at half-maximum of 110 ps. Each experimental TRPL data for Figure 2 were fitted with a convolution of the Gaussian function and the exponential decay ($k = \exp(-\frac{t}{\tau})$). τ for the best fitting at each gate voltage are listed in Supporting Information, Table S2. The values in Supporting Information, Table S2, were used for Figure 2b with uncertainties of the Gaussian-exponential fitting, represented by error bars.

ASSOCIATED CONTENT

Supporting Information

The Supporting Information is available free of charge at <https://pubs.acs.org/doi/10.1021/acsnano.1c04331>.

Figures and sections providing detailed information on quantum yield and carrier density calibration, PL power-dependence, diffusion calculation, nonradiative decay process from a diffusion model, and characterization of IGS (PDF)

AUTHOR INFORMATION

Corresponding Authors

James Hone – Department of Mechanical Engineering, Columbia University, New York, New York 10027, United States; Email: jh2228@columbia.edu

Katayun Barmak – Department of Applied Physics and Applied Mathematics, Columbia University, New York, New York 10027, United States; Email: kb2612@columbia.edu

Xiaoyang Zhu – Department of Chemistry, Columbia University, New York, New York 10027, United States; orcid.org/0000-0002-2090-8484; Email: xz2324@columbia.edu

Authors

Bumho Kim – Department of Mechanical Engineering, Columbia University, New York, New York 10027, United States; orcid.org/0000-0002-5671-5641

Yue Luo – Department of Physics, Stevens Institute of Technology, Hoboken, New Jersey 07030, United States; Center for Nanoscale Systems and Department of Physics, Harvard University, Cambridge, Massachusetts 02138, United States; orcid.org/0000-0002-2757-5395

Daniel Rhodes – Department of Mechanical Engineering, Columbia University, New York, New York 10027, United States; orcid.org/0000-0002-7651-3211

Yusong Bai – Department of Chemistry, Columbia University, New York, New York 10027, United States

Jue Wang – Department of Chemistry, Columbia University, New York, New York 10027, United States; orcid.org/0000-0001-6843-9771

Song Liu – Department of Mechanical Engineering, Columbia University, New York, New York 10027, United States

Abraham Jordan – Department of Chemistry, Columbia University, New York, New York 10027, United States; orcid.org/0000-0002-4343-5675

Baili Huang – Department of Applied Physics and Applied Mathematics, Columbia University, New York, New York 10027, United States

Zhaochen Li – Department of Applied Physics and Applied Mathematics, Columbia University, New York, New York 10027, United States

Takashi Taniguchi – International Center for Materials Nanoarchitectonics, National Institute for Materials Science, Tsukuba 305-0044, Japan; orcid.org/0000-0002-1467-3105

Kenji Watanabe – Research Center for Functional Materials, National Institute for Materials Science, Tsukuba 305-0044, Japan; orcid.org/0000-0003-3701-8119

Jonathan Owen – Department of Chemistry, Columbia University, New York, New York 10027, United States; orcid.org/0000-0001-5502-3267

Stefan Strauf – Department of Physics, Stevens Institute of Technology, Hoboken, New Jersey 07030, United States

Complete contact information is available at:

<https://pubs.acs.org/doi/10.1021/acsnano.1c04331>

Author Contributions

J.H., X.Z., D.R., and B.K. designed the experiment. B.K., D.R., and S.L. performed crystal growth. D.R. and S.L. measured STM topographic images. B.K., B.H., and Z.L. made stacks of the heterostructure. B.K. fabricated the devices. B.K. and Y.L. carried out QY and lifetime measurements. B.K. and Y.B. performed gate-dependent PL measurements. J.W. conducted

spatial mapping measurement. B.K. proposed the diffusion model for nonradiative decay. T.T. and K.W. provided *h*-BN crystals. S.S., X.Z., K.B., and J.H. supervised experimental work, data collection, and analysis. J.H. and B.K. wrote the manuscript with help from all authors.

Notes

The authors declare no competing financial interest.

ACKNOWLEDGMENTS

Materials synthesis, sample fabrication, diffusion measurements, and data analysis were supported by the NSF MRSEC program through Columbia in the Center for Precision Assembly of Superstratic and Superatomic Solids (DMR-1420634) and the Center for Precision-Assembled Quantum Materials (DMR-2011738). Quantum yield and lifetime measurements were supported by the National Science Foundation (NSF) under award DMR-1809235 (Stevens Institute of Technology, S.S. and Y.L.) and DMR-1809361 (Columbia University, J.H.). STM characterization was supported by U.S. Department of Energy, Office of Science, Basic Energy Sciences, under award no. DESC0019481 (S.L., J.H.). X.Z. acknowledges support by the National Science Foundation (DMR-1809680), for supporting the construction of the confocal fluorescence microscope. Synthesis of BN was supported by the Elemental Strategy Initiative conducted by the MEXT, Japan, grant no. JPMXP0112101001, JSPS KAKENHI grant nos. JP20H00354 and the CREST (JPMJCR15F3), JST (K.W. and T.T.). We thank Kin Fai Mak, Xavier Marie, Yeongsu Cho, and Timothy C. Berkelbach for useful discussions.

REFERENCES

- (1) Mak, K. F.; Lee, C.; Hone, J.; Shan, J.; Heinz, T. F. Atomically Thin MoS_2 : A New Direct-Gap Semiconductor. *Phys. Rev. Lett.* **2010**, *105*, 136805.
- (2) Chernikov, A.; Berkelbach, T. C.; Hill, H. M.; Rigosi, A.; Li, Y.; Aslan, O. B.; Reichman, D. R.; Hybertsen, M. S.; Heinz, T. F. Exciton Binding Energy and Nonhydrogenic Rydberg Series in Monolayer WS_2 . *Phys. Rev. Lett.* **2014**, *113*, 076802.
- (3) Ross, J. S.; Wu, S.; Yu, H.; Ghimire, N. J.; Jones, A. M.; Aivazian, G.; Yan, J.; Mandrus, D. G.; Xiao, D.; Yao, W.; Xu, X. Electrical Control of Neutral and Charged Excitons in a Monolayer Semiconductor. *Nat. Commun.* **2013**, *4*, 1474.
- (4) Mak, K. F.; He, K.; Lee, C.; Lee, G. H.; Hone, J.; Heinz, T. F.; Shan, J. Tightly Bound Trions in Monolayer MoS_2 . *Nat. Mater.* **2013**, *12*, 207–211.
- (5) Ye, Z.; Waldecker, L.; Ma, E. Y.; Rhodes, D.; Antony, A.; Kim, B.; Zhang, X.-X.; Deng, M.; Jiang, Y.; Lu, Z.; et al. Efficient Generation of Neutral and Charged Biexcitons in Encapsulated WSe_2 Monolayers. *Nat. Commun.* **2018**, *9*, 3718.
- (6) Pei, J.; Yang, J.; Wang, X.; Wang, F.; Mokkapat, S.; Lü, T.; Zheng, J.-C.; Qin, Q.; Neshev, D.; Tan, H. H.; Jagadish, C.; Lu, Y. Excited State Biexcitons in Atomically Thin MoSe_2 . *ACS Nano* **2017**, *11*, 7468–7475.
- (7) Hao, K.; Specht, J. F.; Nagler, P.; Xu, L.; Tran, K.; Singh, A.; Dass, C. K.; Schüller, C.; Korn, T.; Richter, M.; Knorr, A.; Li, X.; Moody, G.; et al. Neutral and Charged Inter-Valley Biexcitons in Monolayer MoSe_2 . *Nat. Commun.* **2017**, *8*, 15552.
- (8) You, Y.; Zhang, X.-X.; Berkelbach, T. C.; Hybertsen, M. S.; Reichman, D. R.; Heinz, T. F. Observation of Biexcitons in Monolayer WSe_2 . *Nat. Phys.* **2015**, *11*, 477–481.
- (9) Li, Z.; Wang, T.; Lu, Z.; Jin, C.; Chen, Y.; Meng, Y.; Lian, Z.; Taniguchi, T.; Watanabe, K.; Zhang, S.; et al. Revealing the Biexciton and Trion-Exciton Complexes in BN Encapsulated WSe_2 . *Nat. Commun.* **2018**, *9*, 3719.
- (10) Chen, S.-Y.; Goldstein, T.; Taniguchi, T.; Watanabe, K.; Yan, J. Coulomb-Bound Four- and Five-Particle Intervalley States in an Atomically-Thin Semiconductor. *Nat. Commun.* **2018**, *9*, 3717.
- (11) Barbone, M.; Montblanch, A. R.-P.; Kara, D. M.; Palacios-Berraquero, C.; Cadore, A. R.; De Fazio, D.; Pingault, B.; Mostaani, E.; Li, H.; Chen, B.; et al. Charge-Tuneable Biexciton Complexes in Monolayer WSe_2 . *Nat. Commun.* **2018**, *9*, 3721.
- (12) Cotlet, O.; Pientka, F.; Schmidt, R.; Zarand, G.; Demler, E.; Imamoglu, A. Transport of Neutral Optical Excitations Using Electric Fields. *Physical Review X* **2019**, *9*, 041019.
- (13) Yu, H.; Cui, X.; Xu, X.; Yao, W. Valley Excitons in Two-Dimensional Semiconductors. *National Science Review* **2015**, *2*, 57–70.
- (14) Berkelbach, T. C.; Hybertsen, M. S.; Reichman, D. R. Theory of Neutral and Charged Excitons in Monolayer Transition Metal Dichalcogenides. *Phys. Rev. B* **2013**, *88*, 045318.
- (15) Efimkin, D. K.; MacDonald, A. H. Many-Body Theory of Trion Absorption Features in Two-Dimensional Semiconductors. *Phys. Rev. B* **2017**, *95*, 035417.
- (16) Sidler, M.; Back, P.; Cotlet, O.; Srivastava, A.; Fink, T.; Kroner, M.; Demler, E.; Imamoglu, A. Fermi Polaron-Polaritons in Charge-Tunable Atomically Thin Semiconductors. *Nat. Phys.* **2017**, *13*, 255–261.
- (17) Efimkin, D. K.; Laird, E. K.; Levinsen, J.; Parish, M. M.; MacDonald, A. H. Electron-Exciton Interactions in the Exciton-Polaron Problem. *Phys. Rev. B* **2021**, *103*, 075417.
- (18) Rana, F.; Koksai, O.; Manolatu, C. Many-Body Theory of the Optical Conductivity of Excitons and Trions in Two-Dimensional Materials. *Phys. Rev. B* **2020**, *102*, 085304.
- (19) Chang, Y.-W.; Reichman, D. R. Many-Body Theory of Optical Absorption in Doped Two-Dimensional Semiconductors. *Phys. Rev. B* **2019**, *99*, 125421.
- (20) Van Tuan, D.; Jones, A. M.; Yang, M.; Xu, X.; Dery, H. Virtual Trions in the Photoluminescence of Monolayer Transition-Metal Dichalcogenides. *Phys. Rev. Lett.* **2019**, *122*, 217401.
- (21) Lien, D.-H.; Uddin, S. Z.; Yeh, M.; Amani, M.; Kim, H.; Ager, J. W.; Yablonovitch, E.; Javey, A. Electrical Suppression of All Nonradiative Recombination Pathways in Monolayer Semiconductors. *Science* **2019**, *364*, 468–471.
- (22) Ren, T.; Song, P.; Chen, J.; Loh, K. P. Whisper Gallery Modes in Monolayer Tungsten Disulfide-Hexagonal Boron Nitride Optical Cavity. *ACS Photonics* **2018**, *5*, 353–358.
- (23) Yuan, L.; Huang, L. Exciton Dynamics and Annihilation in WS_2 2D Semiconductors. *Nanoscale* **2015**, *7*, 7402–7408.
- (24) Amani, M.; Lien, D.-H.; Kiriya, D.; Xiao, J.; Azcatl, A.; Noh, J.; Madhupraty, S. R.; Addou, R.; Kc, S.; Dubey, M.; Cho, K.; Wallace, R. M.; Lee, S.-C.; He, J.-H.; Ager, J. W.; Zhang, X.; Yablonovitch, E.; Javey, A. Near-Unity Photoluminescence Quantum Yield in MoS_2 . *Science* **2015**, *350*, 1065–1068.
- (25) Kim, H.; Ahn, G. H.; Cho, J.; Amani, M.; Mastandrea, J. P.; Groschner, C. K.; Lien, D.-H.; Zhao, Y.; Ager, J. W.; Scott, M. C.; et al. Synthetic WSe_2 Monolayers with High Photoluminescence Quantum Yield. *Science Advances* **2019**, *5*, No. eaau4728.
- (26) Robert, C.; Lagarde, D.; Cadiz, F.; Wang, G.; Lassagne, B.; Amand, T.; Balocchi, A.; Renucci, P.; Tongay, S.; Urbaszek, B.; Marie, X. Exciton Radiative Lifetime in Transition Metal Dichalcogenide Monolayers. *Phys. Rev. B* **2016**, *93*, 205423.
- (27) Wang, G.; Bouet, L.; Lagarde, D.; Vidal, M.; Balocchi, A.; Amand, T.; Marie, X.; Urbaszek, B. Valley Dynamics Probed through Charged and Neutral Exciton Emission in Monolayer WSe_2 . *Phys. Rev. B* **2014**, *90*, 075413.
- (28) Lorchat, E.; López, L. E. P.; Robert, C.; Lagarde, D.; Froehlicher, G.; Taniguchi, T.; Watanabe, K.; Marie, X.; Berciaud, S. Filtering the Photoluminescence Spectra of Atomically Thin Semiconductors with Graphene. *Nat. Nanotechnol.* **2020**, *15*, 283–288.
- (29) Sanvitto, D.; Pulizzi, F.; Shields, A. J.; Christianen, P. C. M.; Holmes, S. N.; Simmons, M. Y.; Ritchie, D. A.; Maan, J. C.; Pepper,

M. Observation of Charge Transport by Negatively Charged Excitons. *Science* **2001**, 294, 837–839.

(30) Cadiz, F.; Robert, C.; Courtade, E.; Manca, M.; Martinelli, L.; Taniguchi, T.; Watanabe, K.; Amand, T.; Rowe, A. C. H.; Paget, D.; et al. Exciton Diffusion in WSe₂ Monolayers Embedded in a van der Waals Heterostructure. *Appl. Phys. Lett.* **2018**, 112, 152106.

(31) Kato, T.; Kaneko, T. Transport Dynamics of Neutral Excitons and Trions in Monolayer WS₂. *ACS Nano* **2016**, 10, 9687–9694.

(32) Edelberg, D.; Rhodes, D.; Kerelsky, A.; Kim, B.; Wang, J.; Zangiabadi, A.; Kim, C.; Abhinandan, A.; Ardelean, J.; Scully, M.; Scullion, D.; Embon, L.; Zu, R.; Santos, E. J. G.; Balicas, L.; Marianetti, C.; Barmak, K.; Zhu, X.; Hone, J.; Pasupathy, A. N. Approaching the Intrinsic Limit in Transition Metal Diselenides via Point Defect Control. *Nano Lett.* **2019**, 19, 4371–4379.

(33) Hong, J.; Hu, Z.; Probert, M.; Li, K.; Lv, D.; Yang, X.; Gu, L.; Mao, N.; Feng, Q.; Xie, L.; et al. Exploring Atomic Defects in Molybdenum Disulfide Monolayers. *Nat. Commun.* **2015**, 6, 6293.

(34) Coelho, P. M.; Komsa, H.-P.; Coy Diaz, H.; Ma, Y.; Krashenninnikov, A. V.; Batzill, M. Post-Synthesis Modifications of Two-Dimensional MoSe₂ or MoTe₂ by Incorporation of Excess Metal Atoms into the Crystal Structure. *ACS Nano* **2018**, 12, 3975–3984.

(35) Ajayi, O. A.; Ardelean, J. V.; Shepard, G. D.; Wang, J.; Antony, A.; Taniguchi, T.; Watanabe, K.; Heinz, T. F.; Strauf, S.; Zhu, X.-Y.; Hone, J. C. Approaching the Intrinsic Photoluminescence Linewidth in Transition Metal Dichalcogenide Monolayers. *2D Materials* **2017**, 4, 031011.

(36) Dean, C. R.; Young, A. F.; Meric, I.; Lee, C.; Wang, L.; Sorgenfrei, S.; Watanabe, K.; Taniguchi, T.; Kim, P.; Shepard, K. L.; Hone, J. Boron Nitride Substrates for High-Quality Graphene Electronics. *Nat. Nanotechnol.* **2010**, 5, 722–726.

(37) Shepard, G. D.; Ardelean, J. V.; Ajayi, O. A.; Rhodes, D.; Zhu, X.; Hone, J. C.; Strauf, S. Trion-Species-Resolved Quantum Beats in MoSe₂. *ACS Nano* **2017**, 11, 11550–11558.

(38) Zhou, Y.; Scuri, G.; Wild, D. S.; High, A. A.; Dibos, A.; Jauregui, L. A.; Shu, C.; De Greve, K.; Pistunova, K.; Joe, A. Y.; et al. Probing Dark Excitons in Atomically Thin Semiconductors via Near-Field Coupling to Surface Plasmon Polaritons. *Nat. Nanotechnol.* **2017**, 12, 856–860.

(39) Kümmell, T.; Quitsch, W.; Matthis, S.; Litwin, T.; Bacher, G. Gate Control of Carrier Distribution in k-Space in MoS₂ Monolayer and Bilayer Crystals. *Phys. Rev. B* **2015**, 91, 125305.

(40) Rana, F.; Koksai, O.; Jung, M.; Shvets, G.; Manolatu, C. Many-Body Theory of Radiative Lifetimes of Exciton-Trion Superposition States in Doped Two-Dimensional Materials. *Phys. Rev. B* **2021**, 103, 035424.

(41) Wang, G.; Palleau, E.; Amand, T.; Tongay, S.; Marie, X.; Urbaszek, B. Polarization and Time-Resolved Photoluminescence Spectroscopy of Excitons in MoSe₂ Monolayers. *Appl. Phys. Lett.* **2015**, 106, 112101.

(42) Hao, K.; Xu, L.; Nagler, P.; Singh, A.; Tran, K.; Dass, C. K.; Schüller, C.; Korn, T.; Li, X.; Moody, G. Coherent and Incoherent Coupling Dynamics between Neutral and Charged Excitons in Monolayer MoSe₂. *Nano Lett.* **2016**, 16, S109–S113.

(43) Titze, M.; Li, B.; Zhang, X.; Ajayan, P. M.; Li, H. Intrinsic Coherence Time of Trions in Monolayer MoSe₂ Measured via Two-Dimensional Coherent Spectroscopy. *Physical Review Materials* **2018**, 2, 054001.

(44) Wang, H.; Zhang, C.; Chan, W.; Manolatu, C.; Tiwari, S.; Rana, F. Radiative Lifetimes of Excitons and Trions in Monolayers of the Metal Dichalcogenide MoS₂. *Phys. Rev. B* **2016**, 93, 045407.

(45) Fang, H.; Han, B.; Robert, C.; Semina, M.; Lagarde, D.; Courtade, E.; Taniguchi, T.; Watanabe, K.; Amand, T.; Urbaszek, B.; Glazov, M.; Marie, X. Control of the Exciton Radiative Lifetime in van der Waals Heterostructures. *Phys. Rev. Lett.* **2019**, 123, 067401.

(46) Cotlet, O.; Pientka, F.; Schmidt, R.; Zarand, G.; Demler, E.; Imamoglu, A. Transport of Neutral Optical Excitations Using Electric Fields. *Physical Review X* **2019**, 9, 041019.

(47) Palummo, M.; Bernardi, M.; Grossman, J. C. Exciton Radiative Lifetimes in Two-Dimensional Transition Metal Dichalcogenides. *Nano Lett.* **2015**, 15, 2794–2800.

(48) Goodman, A. J.; Willard, A. P.; Tisdale, W. A. Exciton Trapping is Responsible for the Long Apparent Lifetime in Acid-Treated MoS₂. *Phys. Rev. B* **2017**, 96, 121404.

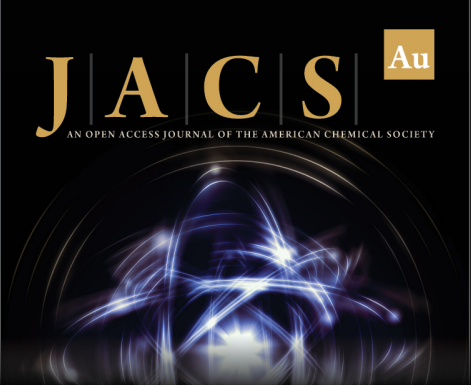
(49) Paur, M.; Molina-Mendoza, A. J.; Bratschitsch, R.; Watanabe, K.; Taniguchi, T.; Mueller, T. Electroluminescence from Multi-Particle Exciton Complexes in Transition Metal Dichalcogenide Semiconductors. *Nat. Commun.* **2019**, 10, 1709.

(50) Withers, F.; Del Pozo-Zamudio, O.; Mishchenko, A.; Rooney, A. P.; Gholinia, A.; Watanabe, K.; Taniguchi, T.; Haigh, S. J.; Geim, A. K.; Tartakovskii, A. I.; Novoselov, K. S. Light-Emitting Diodes by Band-Structure Engineering in van der Waals Heterostructures. *Nat. Mater.* **2015**, 14, 301–306.


(51) Britnell, L.; Ribeiro, R. M.; Eckmann, A.; Jalil, R.; Belle, B. D.; Mishchenko, A.; Kim, Y.-J.; Gorbachev, R. V.; Georgiou, T.; Morozov, S. V.; Grigorenko, A. N.; Geim, A. K.; Casiraghi, C.; Neto, A. H. C.; Novoselov, K. S. Strong Light-Matter Interactions in Heterostructures of Atomically Thin Films. *Science* **2013**, 340, 1311–1314.


(52) Son, S.; Shin, Y. J.; Zhang, K.; Shin, J.; Lee, S.; Idzuchi, H.; Coak, M. J.; Kim, H.; Kim, J.; Kim, J. H.; Kim, M.; Kim, D.; Kim, P.; Park, J.-G. Strongly Adhesive Dry Transfer Technique for van der Waals Heterostructure. *2D Materials* **2020**, 7, 041005.


(53) Wang, L.; Meric, I.; Huang, P. Y.; Gao, Q.; Gao, Y.; Tran, H.; Taniguchi, T.; Watanabe, K.; Campos, L. M.; Muller, D. A.; Guo, J.; Kim, P.; Hone, J.; Shepard, K. L.; Dean, C. R. One-Dimensional Electrical Contact to a Two-Dimensional Material. *Science* **2013**, 342, 614–617.



JACS Au
AN OPEN ACCESS JOURNAL OF THE AMERICAN CHEMICAL SOCIETY

 Editor-in-Chief
Prof. Christopher W. Jones
Georgia Institute of Technology, USA

Open for Submissions 

pubs.acs.org/jacsau  ACS Publications
Most Trusted. Most Cited. Most Read.